Gauge Dependence of the $\tilde{S}$ Molecular Orbital Space Decomposition of Optical Rotation

Ty Balduf · Marco Caricato

October 28, 2020

Abstract Optical rotation (OR) is a foundational technique for the detection and characterization of chiral molecules, but it is poorly understood how the observed property relates to the structure of the molecule. Over the years, several schemes have been developed to decompose the OR into more chemically intuitive contributions. In this paper, we introduce two alternative formulations of our previously developed $\tilde{S}$ molecular orbital space decomposition. These new expressions use the Modified Velocity Gauge-Magnetic (MVG-M) and -Electric (MVG-E) definitions of OR, rather than the Length Gauge-Magnetic (LG-M) definition used in the original paper. Comparing these formulations across a small set of previously studied chiral molecules, we find that these different definitions produce consistent physical interpretations of the OR. These results further confirm the robustness of the $\tilde{S}$ methodology for the investigation of structure-property relationships in chiral molecules.

Keywords Optical Rotation · Gauge Dependence · Response Theory · Orbital Decomposition

1 Introduction

Detecting and controlling molecular and supra-molecular chirality is an active area of research with applications ranging from pharmaceutical development [1] and organic chiral catalysis [2, 3, 4] to nanostructure assembly [5, 6] and chiral light generation [7, 8]. Optical rotation (OR), the change in orientation of plane polarized light

Marco Caricato
Department of Chemistry, University of Kansas, 1567 Irving Hill Road, Lawrence, Kansas 66045, United States
E-mail: mcaricato@ku.edu

impinging on a chiral sample, is a foundational technique for absolute configuration assignment and chiral sensing [9, 10, 11, 12]. Despite the long standing use of OR measurements, the relationship between the structural features of a compound and its observed OR remains unclear.

In recent years, a number of theoretical schemes have been developed to decompose the OR into electronic contributions in an effort to understand how the molecular shape affects the OR. Wiberg et al. have used the sum-over-states formulation to describe OR contributions in terms of movement of charge density in excited state transitions [13]. Polavarapu et al. used modern electronic structure methods to test the semiempirical Kirkwood model, which expresses the OR as a sum of bond polarizabilities and anisotropies [14, 15]. Beratan et al. developed a Mulliken-like partitioning to assign OR contributions to individual atoms and functional groups of a molecule [16]. Autschbach et al. studied how OR could be split into molecular orbital (MO) contributions [17].

We previously proposed a similar method to Autschbach et al. where instead of assigning contributions to individual MOs, we instead decompose the OR into contributions from occupied to virtual MO transitions [18]. We refer to these contributions as $\tilde{S}_{ia}$ values, where i/a is the index of an occupied/virtual MO pair. While a molecule can have many possible transitions, the OR can often be described qualitatively using just the transitions with the largest $\tilde{S}_{ia}$ values. In this way, the induced OR can be ascribed to the movement of electronic density during these transitions. These shifts in the density can be tied to particular functional groups of the molecule, offering chemical intuition that can be applied more generally to other systems. We have used this approach to explain differences in OR between molecular

conformers [19], as well to determine the effect of functionalization [20].

In these prior studies, $\tilde{S}_{ia}$ was expressed in the length gauge (LG), which is a commonly used form for OR calculations. In principle, the choice of gauge should not affect the OR, but this is only true for variational electronic structure methods using an infinite basis and so practical calculations of OR exhibit gauge dependence [21]. Even ignoring these differences in the total OR, there is no guarantee that $\tilde{S}_{ia}$ contributions and their corresponding physical interpretations remain the same if a different gauge is used to define $\tilde{S}$. To address this ambiguity, here we develop two new definitions of $\tilde{S}_{ia}$ with the modified velocity gauge (MVG) and apply them to a subset of the molecules from these prior studies. By comparing among these different definitions, we can determine if they produce consistent physical interpretations of the OR.

This paper is organized as follows. Section 2 gives a brief description of the various definitions that can be used to calculate optical rotation and its MO space decomposition, $\tilde{S}$. Section 3 defines $\hat{S}$ values, a normalized version of $\tilde{S}$, and describes the model chemistry used in our electronic structure calculations. In Section 4, we compute $\hat{S}$ values for a small test set of molecules and analyze how the values change with the choice of gauge/perturbation. We conclude with a discussion of the use of $\tilde{S}$ as an interpretive tool and whether insights from this method are dependent on the choice of definition in Section 5.

2 Theory

The specific rotation $[\alpha]_\omega$ (deg [dm (g/mL)]$^{-1}$) induced by light of frequency ω impinging on an isotropically dispersed chiral sample can be calculated as [21, 22, 23]:

$$[\alpha]_\omega = \frac{-(72 \times 10^6)\hbar^2 N_A \omega^2}{c^2 m_e^2 M} \text{Tr}(\boldsymbol{\beta}) \tag{1}$$

where ω is expressed in atomic units, $\hbar$ is the reduced Planck's constant (J s), N_A is Avogadro's number, c is the speed of light (m/s), m_e is the electron rest mass (kg), and M is the molecular mass (amu). In Eq. 1, $\boldsymbol{\beta}$ is the electric dipole-magnetic dipole polarizability (in a.u.):

$$\beta_{\alpha\beta} = 2 \sum_{j \neq 0} \text{Im} \frac{\langle \Psi_0 | \mu_\alpha | \Psi_j \rangle \langle \Psi_j | m_\beta | \Psi_0 \rangle}{\omega_j^2 - \omega^2} \tag{2}$$

The α/β subscripts index Cartesian components of vector/tensor quantities, while j indexes the excited states of the molecule. $\boldsymbol{\mu} = -\boldsymbol{r}$ and $\boldsymbol{m} = \frac{i}{2}(\boldsymbol{r} \times \nabla)$ are respectively the electric and magnetic dipole operators in

atomic units, with the position $\boldsymbol{r}$ and gradient ∇ operators implicitly summed over all the electrons of the molecule.

Eq. (2) is not used in practice, as the sum over excited states is slow to converge [24]. Instead, $\boldsymbol{\beta}$ is typically evaluated via linear response (LR) theory, which for self consistent field (SCF) methods takes the form:[23, 25, 26]

$$\beta_{\alpha\beta} = \frac{1}{c_\omega} \sum_i^{N_{\text{occ}}} \sum_a^{N_{\text{virt}}} \langle \phi_i | \mu_\alpha | \phi_a \rangle \langle \phi_a | X_{m_\beta}^+ | \phi_i \rangle$$
$$= \frac{1}{c_\omega} \sum_i^{N_{\text{occ}}} \sum_a^{N_{\text{virt}}} \langle \phi_i | X_{\mu_\alpha}^- | \phi_a \rangle \langle \phi_a | m_\beta | \phi_i \rangle \tag{3}$$

where $\langle \phi_a | X_{y_\alpha}^\pm | \phi_i \rangle$ represents the density perturbed by the y field (either electric or magnetic) expressed in the molecular orbital (MO) basis, and $c_\omega = \omega$ for LG or $c_\omega = \omega^2$ for MVG (see below). Typically, the expressions in Eq. 3 are actually calculated in atomic orbital basis (AO), but the MO basis is more convenient here for clarity's sake. The perturbed density is computed by solving the linear response equations:

$$\langle \phi_a | X_{y_\alpha}^\pm | \phi_i \rangle = \langle \Phi_i^a | X_{y_\alpha}^\pm | \Phi_0 \rangle$$
$$= \sum_j^{N_{\text{occ}}} \sum_b^{N_{\text{virt}}} \langle \Phi_i^a | (H - E_0 \mp \omega)^{-1} | \Phi_j^b \rangle \langle \Phi_j^b | y_\alpha | \Phi_0 \rangle \tag{4}$$

where H is the molecular Hamiltonian operator, $\phi_{i/a}$ is an occupied/virtual MO, Φ_0 is the unperturbed Slater determinant with energy E_0, and Φ_i^a are singly excited Slater determinants. This changes the problem from determining a large number of excited states to finding a self-consistent response of the density to the applied perturbation. Either type of perturbed density can be determined iteratively by solving the LR-SCF equations starting from the ground state wavefunction; as shown in Eq. 3, the electric and magnetic perturbations are equivalent and will result in the same values for $\boldsymbol{\beta}$.

Electric dipole matrix elements in principle satisfy the hypervirial relationship [27]:

$$\langle \phi_a | \mu_\alpha | \phi_i \rangle = \frac{ie}{m_e \omega_{ia}} \langle \phi_a | p_\alpha | \phi_i \rangle \tag{5}$$

where $\boldsymbol{p}$ is the momentum operator and e is the charge of an electron. However, this relationship does not hold for approximate electronic structure methods with finite basis sets and $\boldsymbol{\beta}$ will differ depending on the gauge used to model the perturbation [28]. Optical rotation calculations are generally done in the length gauge (LG), which uses the form of the dipoles on the left-hand side of Eq. (5), or the modified velocity gauge (MVG), which

uses the form on the right-hand side. Length gauge calculations of OR are not origin invariant, which is typically corrected by using gauge-including atomic orbitals (GIAOs) for SCF methods [29]. However, using GIAOs introduces extra terms into the expression for $\boldsymbol{\beta}$ in Eqs. 3-4. These terms can be incorporated into the magnetic perturbed density via the LR equations in Eq. 4, while they remain separate for the electric perturbed density, thus breaking the symmetry between the two sides of Eq. 3 [30]. On the other hand, the OR in the velocity gauge is origin independent for any electronic structure method, but it contains a spurious static field contribution that needs to be evaluated and subtracted out explicitly (hence the name "modified" velocity gauge) [31].

Recently, we developed a configuration space analysis of the $\boldsymbol{\beta}$ tensor as a tool to determine the underlying electronic processes that induce optical rotation in chiral molecules [18, 19]. We defined a rotatory strength in molecular orbital space, $\tilde{S}_{ia}$, resulting from an occupied to virtual $(i \to a)$ MO transition, which can be written in the length gauge as:

$$\tilde{S}_{ia}^{LG-M} = \text{Im}\left[\langle i|\boldsymbol{\mu}|a\rangle \cdot \langle a|\boldsymbol{X}_{\boldsymbol{m}}^{+}|i\rangle\right] \tag{6}$$

such that:

$$\sum_{ia} \tilde{S}_{ia}^{LG-M} = \omega \text{Tr}(\boldsymbol{\beta}^{LG}) \tag{7}$$

The insight behind this approach is that it allows the optical rotation to be expressed as a sum of contributions from individual transitions: By determining which transitions make a large contribution to the OR, one can make qualitative predictions about how particular changes to the molecular geometry or the electronic density will affect the total OR. The $\tilde{S}$ values in the LG are defined in terms of the magnetic perturbed density in Eq. 6 because GIAOs will introduce additional terms for the electric perturbation, as was the case for $\boldsymbol{\beta}$. Incorporating these terms into an $\tilde{S}_{ia}$ definition is nontrivial, so we forgo consideration of the LG-electric perturbed density for the remainder of this paper.

In this work, we propose two new definitions of the $\tilde{S}$ rotatory strength using the modified velocity gauge:

$$\tilde{S}_{ia}^{MVG-M} = \frac{1}{\omega}\text{Re}\left[\langle i|\boldsymbol{p}|a\rangle \cdot \langle a|\boldsymbol{X}_{\boldsymbol{m}}^{+}|i\rangle\right]$$
$$\tilde{S}_{ia}^{MVG-E} = \frac{1}{\omega}\text{Re}\left[\langle i|\boldsymbol{X}_{\boldsymbol{p}}^{-}|a\rangle \cdot \langle a|\boldsymbol{m}|i\rangle\right] \tag{8}$$

such that:

$$\sum_{ia} \tilde{S}_{ia}^{MVG-M} = \sum_{ia} \tilde{S}_{ia}^{MVG-E} = \omega \text{Tr}(\boldsymbol{\beta}^{MVG}) \tag{9}$$

The unphysical static term is already subtracted out in the expressions in Eq. 8. These two definitions provide the same MVG OR once all contributions are included, but each individual value is different. We can define two separate expressions for $\tilde{S}$ with this choice of gauge because there is no complication due to GIAOs. As for the original $\tilde{S}$ definition in Eq. 6, the computational cost to evaluate all $\tilde{S}_{ia}$ values in Eq. 8 is negligible compared to that of the SCF and LR equations. In fact, evaluating $\tilde{S}$ costs $6N^3$ for the AO→MO transformation of the Cartesian components of the dipole integrals and of the perturbed density matrices.

The main goal of this work is to test whether the three $\tilde{S}$ definitions: LG-M in Eq. 6, and MVG-M and MVG-E in Eq. 8 provide a similar qualitative picture of the OR for chiral molecules in terms of constituent one-electron transitions or whether one definition is preferable to the others.

3 Computational Procedure

To analyze how the choice of gauge and perturbed density affects the $\tilde{S}$ values, we compiled a test set of molecules from previous studies based on the length gauge with the magnetic-perturbed density (LG-M) definition of $\tilde{S}$ in Eq. 6, depicted in Figure 1. The optimized geometries were taken as-is from these prior studies (or references therein) and are recorded here in Tables S1-S9 of the Supporting Information (SI) [13, 20, 32, 33]. For each of these molecules, we calculated the total optical rotation and $\tilde{S}$ using the MVG-M and MVG-E definitions in Eq. 8 and compared them with previous LG-M results. Calculations were performed with the B3LYP/aug-cc-pVDZ model chemistry [34, 35] with a 589.3 nm perturbation wavelength in a development version of the GAUSSIAN suite of programs [36]. Note that while this model chemistry has been shown to be reasonable for calculating OR, we make no effort here to assess its accuracy. Rather, we seek to compare the physical interpretation of $\tilde{S}$ with each perturbed density, regardless of how accurately the OR is described using this method.

The overall OR does not change much for different perturbations, see Table S10 in the SI. However, to ensure that differences in the total OR are not influencing comparisons of $\tilde{S}$, we define a normalized configuration rotatory strength, $\hat{S}$:

$$\hat{S}_{ia} = \frac{\tilde{S}_{ia}}{\sum_{jb} \tilde{S}_{jb}} = \frac{\tilde{S}_{ia}}{\omega \text{Tr}(\boldsymbol{\beta})} \tag{10}$$

where the second equality comes from Eqs. 7 or 9. Since by definition $\sum_{ia} \hat{S}_{ia} = 1$ for each molecule and perturbation type, each $\hat{S}_{ia}$ value gives the relative contribution of that transition to the total OR. The sign of $\hat{S}_{ia}$ is
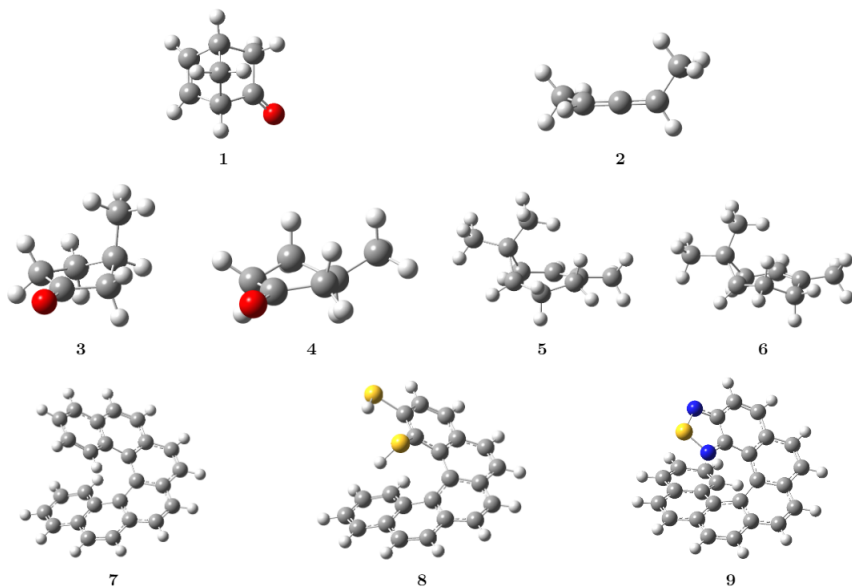
Fig. 1: Structure of the molecules in the test set: (**1**) (1S,4S)-norbornenone, (**2**) P-(2,3)-pentadiene, (**3**,**4**) axial and equatorial (R)-(+)-3-methycyclopentanone, (**5**,**6**) A and B conformers of (S)-(+)-2-carene, (**7**) [6]helicene, (**8**) dithiol[5]helicene, (**9**) benzothiadiazole[6]helicene. Atoms are colored as follows: C (gray), H (white), O (red), N (blue), S (yellow).

positive if $\tilde{S}_{ia}$ has the same sign as $\mathrm{Tr}(\boldsymbol{\beta})$ and negative if $\tilde{S}_{ia}$ has the opposite sign.

4 Results

In this section, we compare $\hat{S}$ values computed with the various perturbed densities for the molecules in Figure 1. To make a comprehensive comparison, we analyze the $\hat{S}$ values of each molecule with increasing level of detail. In Section 4.1, we compare the cumulative contribution to the OR of different sets of $\hat{S}$ values, separated according to their magnitude. In Section 4.2, we use heat maps of $\hat{S}_{ia}$ to visualize how these contributions are distributed among the frontier orbital transitions. From these transitions, we plot the perturbation vectors for the largest contributors in Section 4.3 to determine whether these transitions are consistent across the choice of gauge and perturbed density.

Before delving into these comparisons, we briefly summarize the prior $\tilde{S}$ studies of these molecules. For molecules **1** and **2**, it has been shown that the OR can be qualitatively described by a small fraction of the total number of transitions, coming within an order of magnitude of the total OR with only 3 out of 6583 and 4 out of 3192 $\tilde{S}_{ia}$ values, respectively [18]. The highest occupied molecular orbital (HOMO) to lowest unoccupied molecular orbital (LUMO) transition of molecule **1** is considerably larger than the other transitions and

has the same sign as the overall $\mathrm{Tr}(\boldsymbol{\beta})$, which helps to explain the large OR observed for this molecule. While the four largest magnitude transitions of molecule **2** are comparable in size to the largest transitions of molecule **1**, they come in opposite signed pairs, so their combined contribution is small. This near cancellation provides an explanation for why the observed OR for molecule **2** ($[\alpha]_{355}^{\mathrm{exp}} = 408 \deg [\mathrm{dm} \ (\mathrm{g/mL})]^{-1}$) is significantly smaller than that of molecule **1** ($[\alpha]_{355}^{\mathrm{exp}} = -6310 \deg [\mathrm{dm} \ (\mathrm{g/mL})]^{-1}$).

For molecules **3-6**, $\tilde{S}$ analysis was used to determine the origin of OR differences between conformers [19]. Molecules **3** and **4** each had their largest contribution from the (HOMO→LUMO) transition, but these contributions were opposite in sign, as was the total OR for each conformer. This change in sign was attributed to the electric vector being nearly parallel with the magnetic vector in the axial conformer (**3**), but nearly antiparallel in the equatorial conformer (**4**) due to the change in orientation of the methyl. The difference in OR between molecules **5** and **6** mainly stemmed from differences between HOMO transitions, specifically the (HOMO→LUMO+2) transition. The electric and magnetic vectors for this transition had an angle less than 90° for molecule **5**, but greater than 90° for molecule **6**, resulting in a different sign for the $\tilde{S}_{ia}$ of this transition. For each set of conformers, including transitions within a factor of 10^{-3} of the total sum (30-40% of the transitions) captures 97% of the total OR.

Molecules **7-9** are helicenes, which exhibit a strong chiroptical response due to their axial chirality. $\tilde{S}$ was applied to these molecules and other functionalized helicenes to determine the effect of length and withdrawing/donating character of functional groups on the observed OR [20]. While these molecules have many $\tilde{S}$ contributions, the dominant transitions were characterized by magnetic vectors pointed parallel to the helical axis, which corresponds to electron density moving along the helix body. The magnitude of the magnetic vector for these types of transitions was found to increase with the length of the helix and with delocalization of charge density.

4.1 Cumulative Contribution to the OR

In Figure 2, we plot the cumulative $\hat{S}$ for molecule **1**. On the left hand side, only the largest contributors are included. Moving to the right, progressively smaller contributions are added until all contributions are included and $\sum \hat{S}_{ia} = 1$ for each perturbed density. Scanning across the figure, we can see that the contributions to the OR for each $\hat{S}$ definition become more similar as more transitions are included. The only notable dissimilarity is found in the first set of transitions, where the contribution for the MVG-E definition is half as large as the others. Nevertheless, all $\hat{S}$ definitions require the same number of relevant transitions (2 out of 6583) to provide a qualitative understanding of the OR for this molecule [19]. Once $\hat{S}_{ia}$ values larger in magnitude than 10^{-2} are included in the sum, each $\hat{S}$ definition is no farther than 0.09 from the others. Not only are all the definitions similar at this point in the summation, but they are also within 0.07 of their total sums. Therefore, these results suggest that this MO decomposition of the OR may not be very sensitive to the choice of $\hat{S}$ definition.

Molecules **2-9** also show similarity between the $\hat{S}$ definitions, as depicted in Figure 3. There is some significant variation when only large values are included in the sum, as can be seen for molecule **2**. For the largest magnitude transitions, $|\hat{S}_{ia}| \geq 1$, the LG-M and MVG-M definitions actually have opposite signs compared to their total sums, while the MVG-E definition has the same sign as its total. Note that the four largest transitions do give the correct sign for all the definitions of $\tilde{S}$, consistent with our prior study, but here we have chosen a smaller cutoff for significant contributions and these additional transitions change the sign for the LG-M and MVG-M definitions. For these definitions, there are 7 transitions with $1.0 > |\hat{S}_{ia}| \geq 0.95$, so the choice of cutoff can greatly influence the value and even the sign

of this partial sum. While in this paper we choose consistent cutoffs in order to facilitate comparisons across molecules and $\tilde{S}$ definitions, in practice, the cutoffs used to define significant transitions should be tailored to each molecule. This is clearly exemplified in the case of molecule **2**: the $|\hat{S}_{ia}|$ values for the 4 largest transitions are around an order of magnitude larger than any of the other transitions, which suggests that they should considered separately from the other $|\hat{S}_{ia}| \geq 1$ transitions.

Some of the molecules still have the wrong sign when contributions greater than 10^{-1} are included. For example, the MVG-M definition for **6** is a different sign than the other $\hat{S}$ definitions, though the absolute difference between perturbations is no more than 0.20 in this case. However, once $\hat{S}_{ia}$ contributions larger than 10^{-2} are included, all definitions are qualitatively consistent for all the molecules tested. With $|\hat{S}_{ia}| \geq 10^{-3}$ contributions included, the different $\hat{S}$ definitions are generally indistinguishable.

It is noteworthy that where there are differences between the $\hat{S}$ definitions, the LG-M and MVG-M choices tend to be very similar while MVG-E differs. This is somewhat surprising since the MVG-M and MVG-E definitions are based on the same choice of gauge and produce identical overall OR values. In the next section, we explore whether this trend extends to the level of individual transitions.

4.2 Distribution of Contributions

We have seen up to this point that by summing the same set of transitions, we can obtain a similar proportion of the total OR for each $\hat{S}$ definition. However, the cumulative summation does not show how much individual transitions contribute. To give a more detailed representation of how the OR is distributed among the transitions, we present heat maps of $\hat{S}_{ia}$ in Figures 4-5. As most of the sizable transitions are between frontier orbitals, the heat maps only display transitions among the 15 highest occupied and 15 lowest virtual orbitals. Full maps are reported in Figures S1-S9 of the SI.

Focusing first on **1**, Figure 4 plots its frontier transitions using the LG-M, MVG-M, and MVG-E definitions. The largest two $|\hat{S}_{ia}|$ values for each definition correspond to the (HOMO→LUMO) and (HOMO-1→LUMO) transitions, which are also the transitions included in the first range of Figure 2. However, while these transitions have similar $\hat{S}_{ia}$ for LG-M and MVG-M, they are much smaller for the MVG-E definition (e.g. $\hat{S}_{29,1}$=4.65, 5.12, and 1.84 for the LG-M, MVG-M, and MVG-E definitions respectively). This pattern seems to hold across frontier transitions of **1**, with a
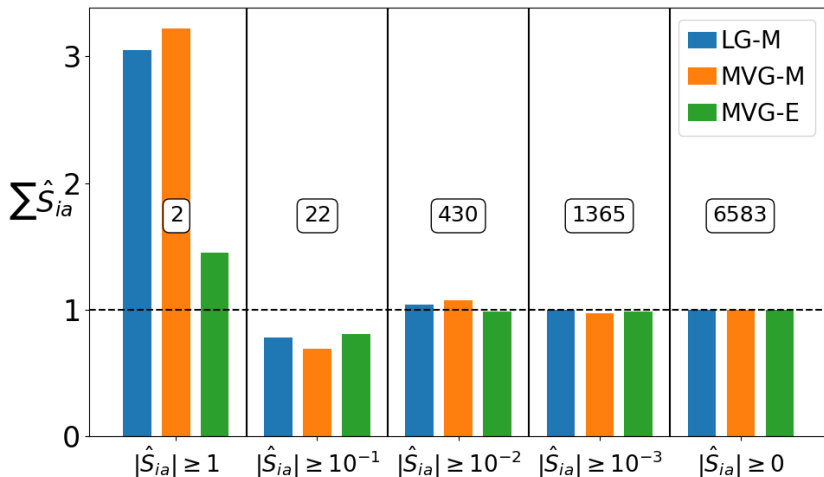
Fig. 2: Cumulative $\hat{S}_{ia}$ for molecule **1** computed with LG-M, MVG-M, and MVG-E definitions. The transitions selected are those for which the LG-M $|\hat{S}_{ia}|$ is greater than the specified value. The height of each bar is the sum of these transitions, while the number of transitions included is listed above the bars.

consistent distribution of $\hat{S}_{ia}$ for each choice of perturbed density, but with smaller magnitudes with the MVG-E choice.

For the rest of the test set, shown in Figure 5, the distribution of $\hat{S}$ among the frontier transitions remains largely unchanged with different $\hat{S}$ definitions. While some of the molecules, such as **2** and **3**, exhibit consistently smaller $\hat{S}$ values with MVG-E than with the other definitions, this is not the case in general. For example, $\hat{S}_{ia}$ values for **5** are similar in magnitude for each definition and the MVG-E choice for **7** actually has some larger transitions than the other definitions, e.g. (HOMO-1→LUMO).

The similarity in the distribution of values for each $\hat{S}$ definition would suggest that $\hat{S}$ is largely invariant to the choice of gauge and perturbed density. However, the differences in magnitude seen for MVG-E could still be a sign that it is producing physically distinct transitions when compared to the magnetic perturbed densities. To resolve this possible ambiguity, we focus on individual transitions and determine whether they produce the same kind of transition for each $\hat{S}$ definition.

4.3 Major Contributions to the OR

To address whether $\hat{S}_{ia}$ has the same physical interpretation with different definitions, we superimpose the electric and magnetic dipole/perturbed density vectors of the largest transitions onto the molecules using the VMD program [37]. These vectors describe how the electronic density rearranges itself to induce OR; similar vectors for a given occupied-virtual transition indi-

cate a similar underlying physical process. The angles between the vectors for the transition considered here are reported in Table S11 of the SI.

The first row of Figure 6 depicts these vectors for **1**, calculated with each $\hat{S}$ definition. It is clear from the figure that the vectors for all types of $\hat{S}$ have the same orientation and involve the same occupied-virtual MO pair, indicating that the process is indeed the same. While the $\hat{S}$ values for LG-M and MVG-M values are very similar in magnitude, the lengths of their vectors differ, see the left and center columns of Figure 6. This is due to the differences in length nearly canceling in the product (i.e. the electric vector is 2.8 times larger for LG-M than MVG-M, but the magnetic vector is 2.6 times smaller). On the other hand, the MVG-E $\hat{S}$ value is smaller because its much shorter magnetic vector length (1.7 times smaller than LG-M, 4.8 times smaller than MVG-M) is not compensated for by the electric vector length (1.3 times smaller than LG-M, 1.9 times larger than MVG-M).

The other molecules exhibit the same qualitative behavior, where the largest $\hat{S}_{ia}$ contributions come from the same transitions independently of the $\hat{S}$ definition. There are some notable differences between the $\hat{S}$ values obtained with the electric and magnetic perturbed density. For instance, for the HOMO→LUMO+4 transition of molecule **2** in the second row of Figure 6, the angle between the vectors for the MVG-M and LG-M $\hat{S}$ type is around 25°, while for the MVG-E type it is 40°. While this is the largest magnitude transition for the MVG-M and LG-M definitions, it is only the second largest for the MVG-E definition. It also has a smaller $|\hat{S}_{ia}|$ value (44 for MVG-M, 20 for MVG-E) despite having a sim-
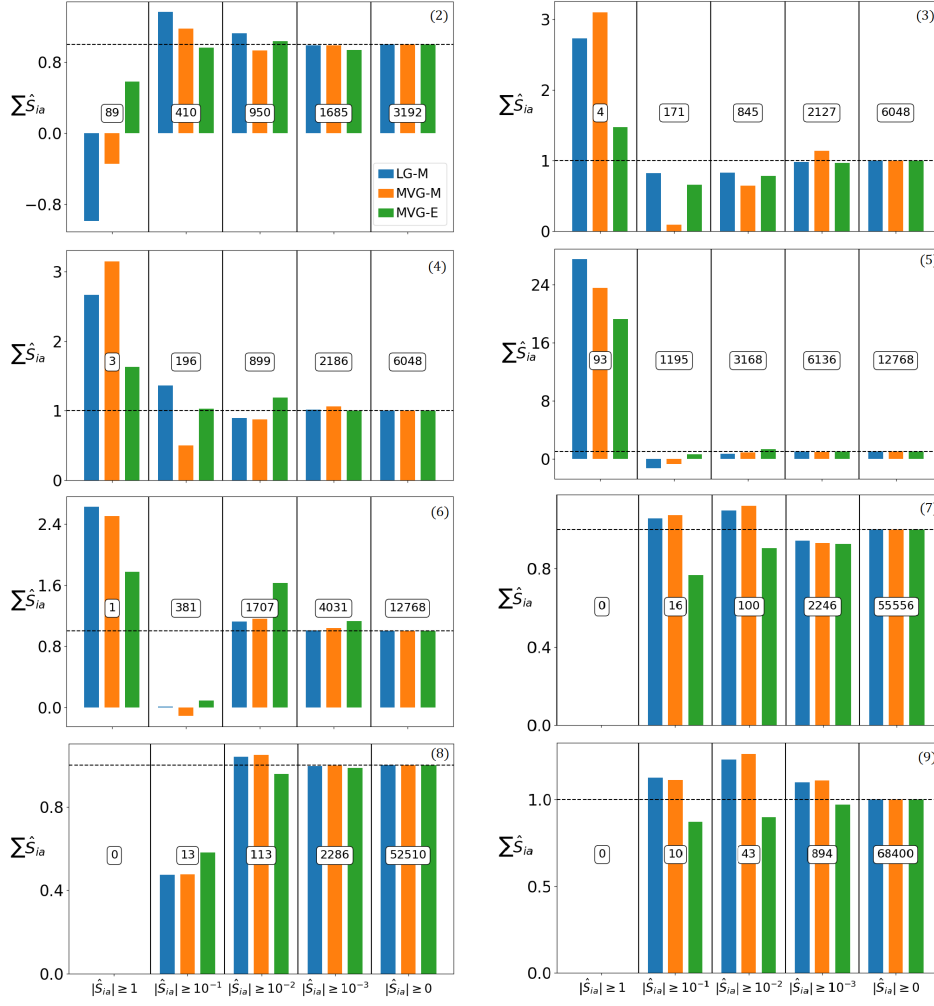
Fig. 3: Cumulative $\hat{S}_{ia}$ for molecules **2-9** computed with LG-M, MVG-M, and MVG-E perturbations. The transitions selected are those for which the LG-M $|\hat{S}_{ia}|$ is greater than the specified value. The height of each bar is the sum of these transitions, while the number of transitions included is listed above the bars. The total sum is marked with a dashed line.
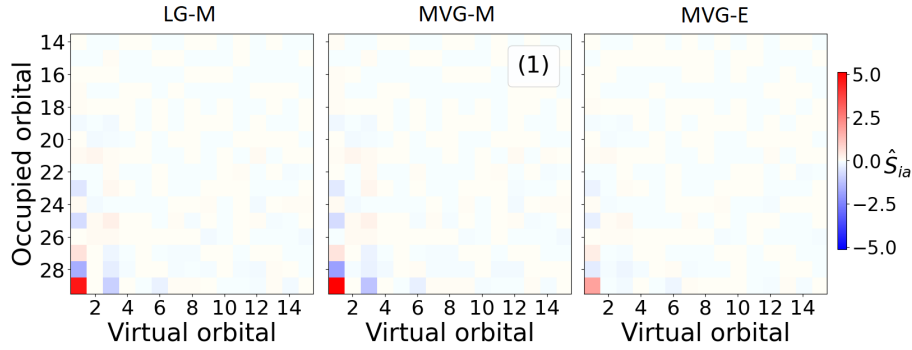

Fig. 4: $\hat{S}_{ia}$ values for the 15 highest occupied and 15 lowest virtual MOs of molecule **1** computed with (from left to right) the LG-M, MVG-M, and MVG-E definitions of $\tilde{S}$.
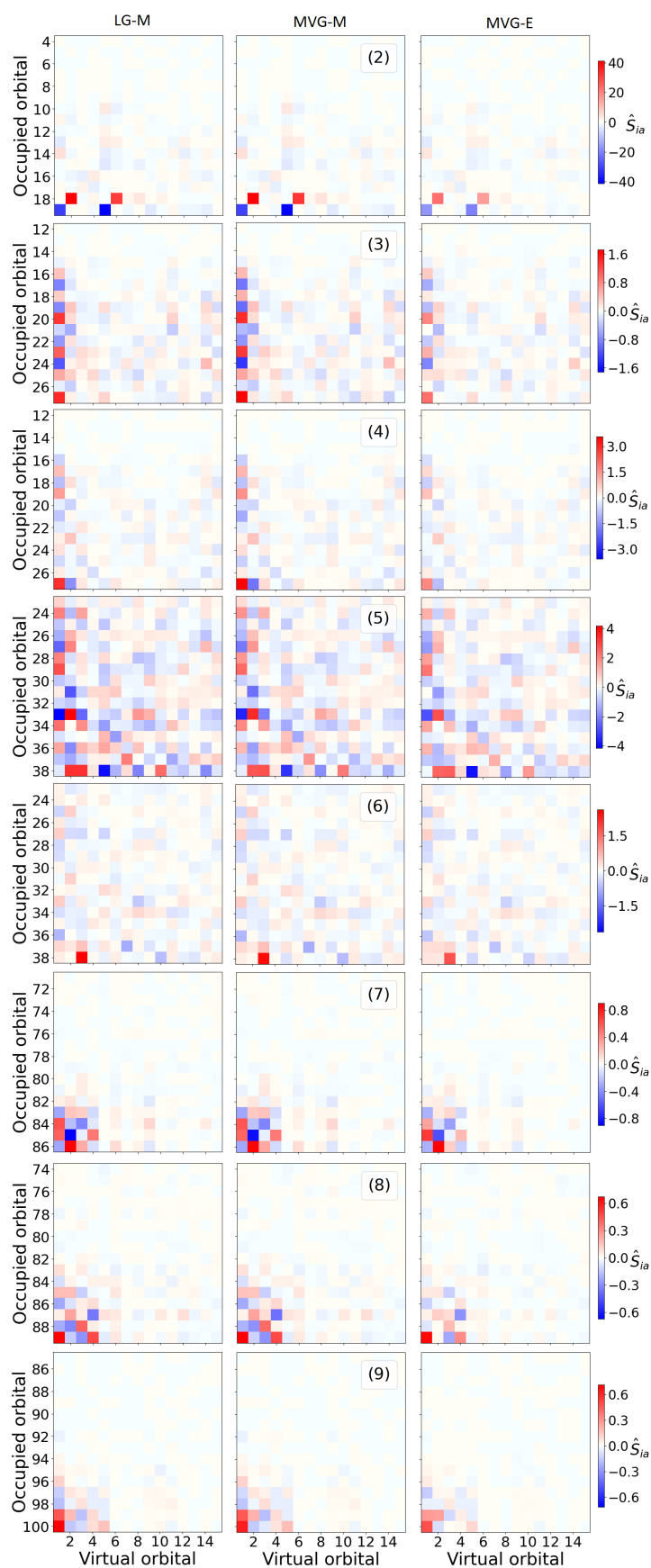
Fig. 5: $\hat{S}_{ia}$ values for the 15 highest occupied and 15 lowest virtual MOs for molecules **2-9** computed with (from left to right) the LG-M, MVG-M, and MVG-E definitions of $\tilde{S}$.
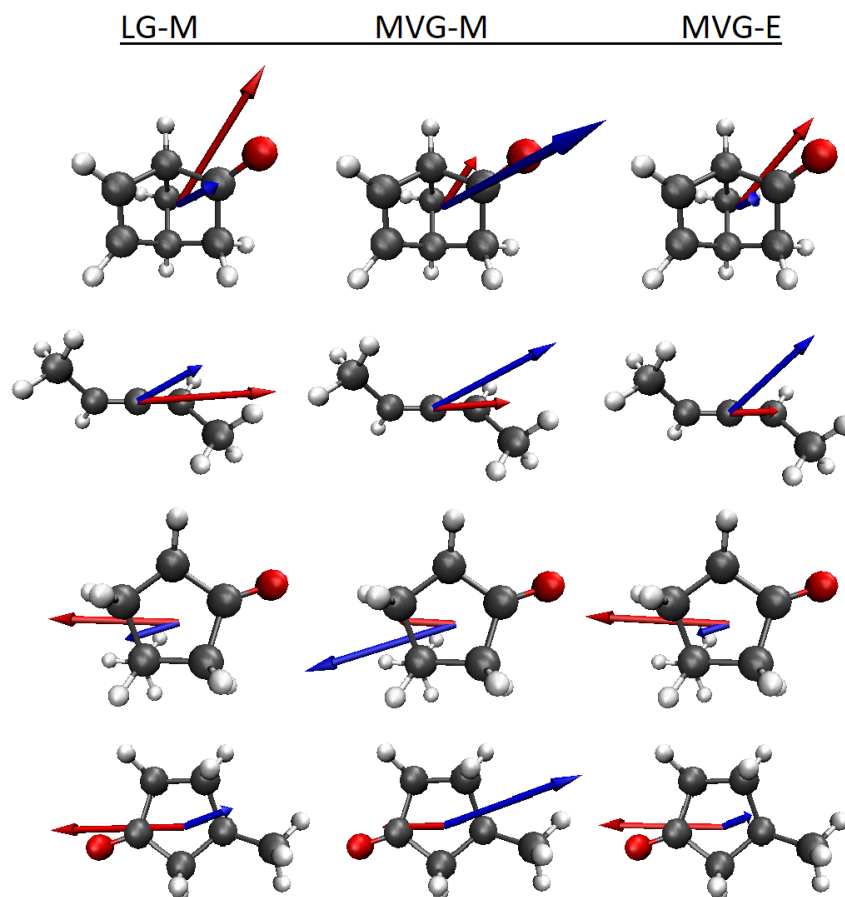
Fig. 6: Electric (red) and magnetic (blue) dipole or perturbed density vectors for the largest transition of molecules **1-4**, computed with (from left to right) the LG-M, MVG-M, and MVG-E definitions of $\tilde{S}$. The transitions depicted are: **1** (HOMO→LUMO), **2** (HOMO→LUMO+4), **3** (HOMO→LUMO), **4** (HOMO→LUMO). For visibility, the length of the the largest electric and magnetic vectors for each molecule is fixed at an arbitrary value and the other vectors are scaled relative to this length.

ilarly sized product of vector magnitudes. Despite this angle difference, the transitions are qualitatively consistent, as the perturbation vectors point essentially in the same direction.

5 Discussion and Conclusions

We have investigated whether different definitions of the $\tilde{S}$ rotatory strength, based on different choices of gauge and perturbed density, provide the same or different pictures for the qualitative description of the optical rotation of chiral molecules. We used a sample of chiral molecules previously studied using the LG-M definition. We find that these different $\tilde{S}$ definitions produce consistent pictures of what physical processes contribute to the optical rotation. This is true at multiple levels of detail. As shown in Section 4.1, partial sums of $\hat{S}$ over selected sets of transitions give similar convergence

to the total OR. Going one level deeper, the distribution of $\hat{S}$ within these sets is mostly the same for each perturbation, as shown in Section 4.2 for the frontier orbital transitions. Finally, at the level of individual transitions, Section 4.3 shows that the largest transitions correspond to the same physical process. Therefore, we posit that $\tilde{S}$ analysis is largely independent of the definition used. However, computing the OR in the modified velocity gauge is approximately twice as costly as in the length gauge, because the MVG approach requires solving the linear response equations both for the desired perturbation frequency and the zero frequency limit. Since the different definitions offer the same interpretation of the OR, the LG-M definition of $\tilde{S}$ may be preferable in terms of the overall computational efficiency of the calculation.
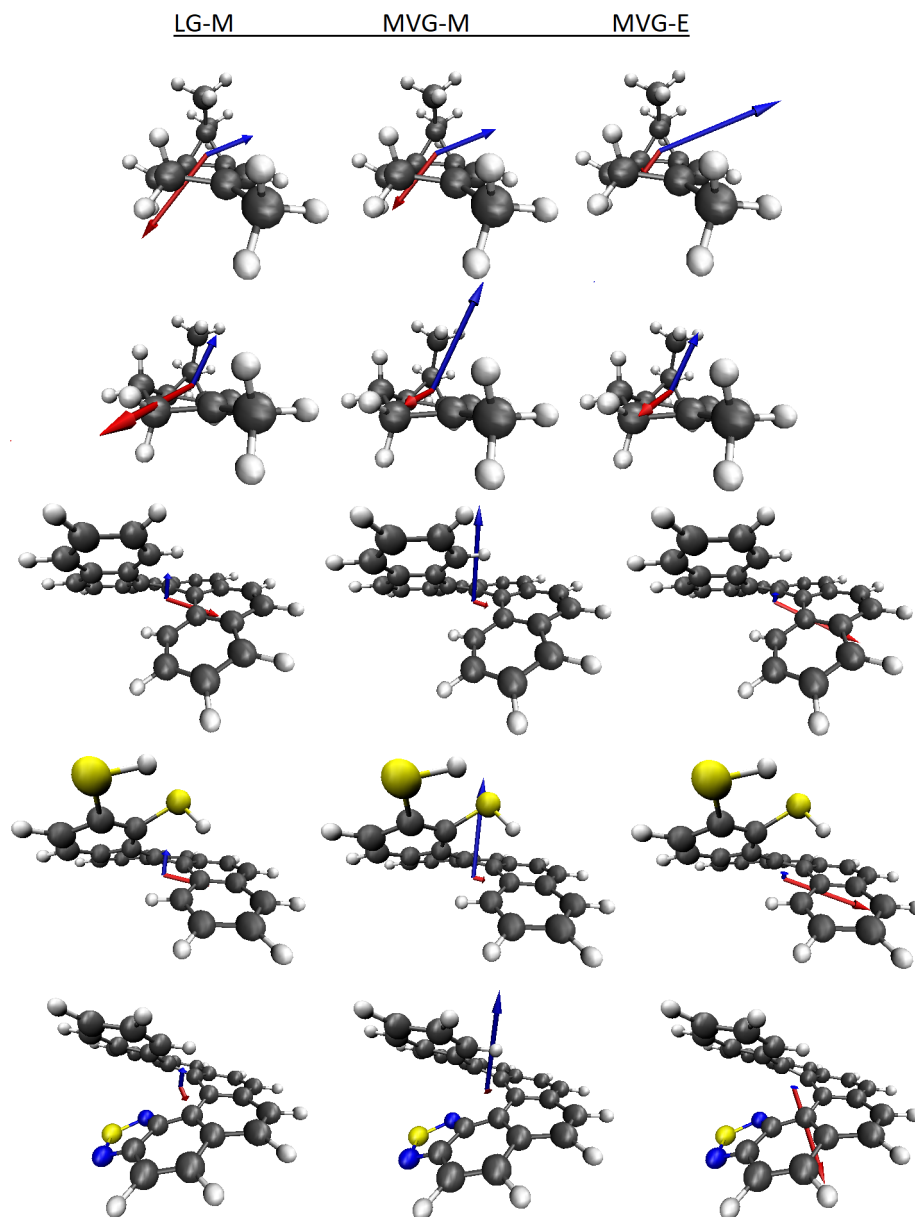
Fig. 7: Electric (red) and magnetic (blue) dipole or perturbed density vectors for the largest transition of molecules **5-9**, computed with (from left to right) the LG-M, MVG-M, and MVG-E definitions of $\tilde{S}$. The transitions depicted are: **5** (HOMO-5→LUMO), **6** (HOMO→LUMO+2), **7** (HOMO→LUMO+1), **8** (HOMO→LUMO), and **9** (HOMO→LUMO). For visibility, the length of the the largest electric and magnetic vectors for each molecule is fixed at an arbitrary value and the other vectors are scaled relative to this length.

Supporting Information

The Supporting Information includes the geometry for each of the molecules discussed in the main text (Tables S1-S9). It also includes the total OR computed with each definition (Table S10), the full heat maps of $\hat{S}_{ia}$ for each of the molecules (Figures S1-S9), and the angles between the vectors of the largest transitions (Table S11).

Conflict of interest

The authors declare that they have no conflict of interest.

References

1. Brooks W, Guida W, Daniel K (2011) The significance of chirality in drug design and development. Curr Top Med Chem 11(7):760–770

2. Hu L, Ren Y, Ramström O (2015) Chirality control in enzyme-catalyzed dynamic kinetic resolution of 1,3-oxathiolanes. J Org Chem 80(16):8478–8481

3. Pfaltz A, Drury WJ (2004) Design of chiral ligands for asymmetric catalysis: From C2-symmetric P,P- and N,N-ligands to sterically and electronically nonsymmetrical P,N-ligands. PNAS 101(16):5723–5726

4. Takata S, Endo Y, Ullah MS, Itsuno S (2016) Synthesis of cinchona alkaloid sulfonamide polymers as sustainable catalysts for the enantioselective desymmetrization of cyclic anhydrides. RSC Adv 2(31):10107–10111

5. Mastroianni AJ, Claridge SA, Alivisatos AP (2009) Pyramidal and chiral groupings of gold nanocrystals assembled using DNA scaffolds. J Am Chem Soc 131(24):8455–8459

6. Liu B, Wu F, Gui H, Zheng M, Zhou C (2017) Chirality-controlled synthesis and applications of single-wall carbon nanotubes. ACS Nano 11(1):31–53

7. Le KQ, Hashiyada S, Kondo M, Okamoto H (2018) Circularly polarized photoluminescence from achiral dye molecules induced by plasmonic two-dimensional chiral nanostructures. J Phys Chem C 122(43):24924–24932

8. Kan Y, Andersen SKH, Ding F, Kumar S, Zhao C, Bozhevolnyi SI (2020) Metasurface-enabled generation of circularly polarized single photons. Adv Mater 32(16):1907832

9. Vaccaro PH (2012) Comprehensive Chiroptical Spectroscopy, Instrumentation, Methodologies, and Theoretical Simulations., 1st edn. John Wiley & Sons;, New York

10. Srivastava N, Macha L, Ha HJ (2019) Total synthesis and stereochemical revision of biemamides B and D. Org Lett 21(22):8992–8996

11. Droulias S, Bougas L (2020) Absolute chiral sensing in dielectric metasurfaces using signal reversals. Nano Lett 20(8):5960–5966

12. Polavarapu PL (1997) Ab initio molecular optical rotations and absolute configurations. Mol Phys 91(3):551–554

13. Wiberg KB, Caricato M, Wang YG, Vaccaro PH (2013) Towards the accurate and efficient calculation of optical rotatory dispersion using augmented minimal basis sets. Chirality 25(10):606–616

14. Polavarapu PL, Chakraborty DK, Ruud K (2000) Molecular optical rotation: An evaluation of semiempirical models. Chem Phys Lett 319(5-6):595–600

15. Kirkwood JG (1937) On the theory of optical rotatory power. J Chem Phys 5(6):479

16. Kondru RK, Wipf P, Beratan DN (1998) Atomic contributions to the optical rotation angle as a quantitative probe of molecular chirality. Science 282(5397):2247–2250

17. Moore B, Srebro M, Autschbach J (2012) Analysis of optical activity in terms of bonds and lone-pairs: The exceptionally large optical rotation of norbornenone. J Chem Theory Comput 8(11):4336–4346

18. Caricato M (2015) Conformational effects on specific rotation: A theoretical study based on the $\tilde{S}_k$ method. J Phys Chem A 119(30):8303–8310

19. Caricato M (2015) Orbital analysis of molecular optical activity based on configuration rotatory strength. J Chem Theory Comput 11(4):1349–1353

20. Aharon T, Caricato M (2019) Configuration space analysis of the specific rotation of helicenes. J Phys Chem A 123(20):4406–4418

21. Crawford TD (2006) Ab initio calculation of molecular chiroptical properties. Theor Chem Acc 115(4):227–245

22. Buckingham AD, Dunn MB (1971) Optical activity of oriented molecules. J Chem Soc Inorg Phys Theor Chem (0):1988–1991

23. Autschbach J, Nitsch-Velasquez L, Rudolph M (2011) Time-dependent density functional response theory for electronic chiroptical properties of chiral molecules. Top Curr Chem 298:1–98

24. Wiberg KB, Wang YG, Wilson SM, Vaccaro PH, Cheeseman JR (2006) Sum-over-states calculation of the specific rotations of some substituted oxiranes, chloropropionitrile, ethane, and norbornenone. J Phys Chem A 110(51):13995–14002

25. McWeeny R (1978) Methods of Molecular Quantum Mechanics, 2nd edn. Academic Press, San Diego

26. Crawford TD, Tam MC, Abrams ML (2007) The current state of ab initio calculations of optical rotation and electronic circular dichroism spectra. J Phys Chem A 111(48):12057–12068

27. Pelloni S, Lazzeretti P (2014) On the determination of the diagonal components of the optical activity tensor in chiral molecules. The Journal of Chemical Physics 140(7):074105

28. Pedersen TB (2012) Introduction to Response Theory. In: Leszczynski J, Kaczmarek-Kedziera A, Papadopoulous MG, Reis H, Sadlej AJ, Manoj K Shukla (eds) Handbook of Computational Chemistry, 1st edn, Springer Reference, Springer Netherlands, pp 135–156

29. Ditchfield R (1974) Self-consistent perturbation theory of diamagnetism I. A gauge-invariant LCAO method for N.M.R. chemical shifts. Mol Phys 27(4):789–807

30. Krykunov M, Autschbach J (2005) Calculation of optical rotation with time-periodic magnetic-field-dependent basis functions in approximate time-dependent density-functional theory. J Chem Phys 123(11):114103

31. Pedersen TB, Koch H, Boman L, Sánchez de Merás AM (2004) Origin invariant calculation of optical rotation without recourse to london orbitals. Chemical Physics Letters 393(4-6):319–326

32. Lahiri P, Wiberg KB, Vaccaro PH (2012) A tale of two carenes: Intrinsic optical activity and large-amplitude nuclear displacement. J Phys Chem A 116(38):9516–9533

33. Lahiri P, Wiberg KB, Vaccaro PH (2013) Intrinsic optical activity and conformational flexibility: The role of size-dependent ring morphology in model cycloketones. J Phys Chem A 117(47):12382–12400

34. Dunning TH (1989) Gaussian basis sets for use in correlated molecular calculations. I. The atoms boron through neon and hydrogen. J Chem Phys 90(2):1007

35. Becke AD (1993) Density-functional thermochemistry. III. The role of exact exchange. J Chem Phys 98(7):5648–5652

36. Frisch MJ, Trucks GW, Schlegel HB, Scuseria GE, Robb MA, Cheeseman JR, Scalmani G, Barone V, Petersson GA, Nakatsuji H, Li X, Caricato M, Marenich AV, Bloino J, Janesko BG, Gomperts R, Mennucci B, Hratchian HP, Ortiz JV, Izmaylov AF, Sonnenberg JL, Williams-Young D, Ding F, Lipparini F, Egidi F, Goings J, Peng B, Petrone A, Henderson T, Ranasinghe D, Zakrzewski VG, Gao J, Rega N, Zheng G, Liang W, Hada M, Ehara M, Toyota K, Fukuda R, Hasegawa J, Ishida M, Nakajima T, Honda Y, Kitao O, Nakai H, Vreven T, Throssell K, Montgomery JA Jr, Peralta JE, Ogliaro F, Bearpark MJ, Heyd JJ, Brothers EN, Kudin KN, Staroverov VN, Keith TA, Kobayashi R, Normand J, Raghavachari K, Rendell AP, Burant JC, Iyengar SS, Tomasi J, Cossi M, Millam JM, Klene M, Adamo C, Cammi R, Ochterski JW, Martin RL, Morokuma K, Farkas O, Foresman JB, Fox DJ (2018) Gaussian Development Version Revision J.02

37. Humphrey W, Dalke A, Schulten K (1996) VMD: Visual molecular dynamics. J Mol Graph 14(1):33–38